

Energy Flow in the Hadronic Final State of Diffractive and Non-Diffractive Deep-Inelastic Scattering at HERA

H1 Collaboration

Abstract:

An investigation of the hadronic final state in diffractive and non-diffractive deep-inelastic electron-proton scattering at HERA is presented, where diffractive data are selected experimentally by demanding a large gap in pseudo-rapidity around the proton remnant direction. The transverse energy flow in the hadronic final state is evaluated using a set of estimators which quantify topological properties. Using available Monte Carlo QCD calculations, it is demonstrated that the final state in diffractive DIS exhibits the features expected if the interaction is interpreted as the scattering of an electron off a current quark with associated effects of perturbative QCD. A model in which deep-inelastic diffraction is taken to be the exchange of a pomeron with partonic structure is found to reproduce the measurements well. Models for deep-inelastic ep scattering, in which a sizeable diffractive contribution is present because of non-perturbative effects in the production of the hadronic final state, reproduce the general tendencies of the data but in all give a worse description.

S. Aid¹⁴, V. Andreev²⁶, B. Andrieu²⁹, R.-D. Appuhn¹², M. Arpagaus³⁷, A. Babaev²⁵, J. Bähr³⁶, J. Bán¹⁸, Y. Ban²⁸, P. Baranov²⁶, E. Barrelet³⁰, R. Barschke¹², W. Bartel¹², M. Barth⁵, U. Bassler³⁰, H.P. Beck³⁸, H.-J. Behrend¹², A. Belousov²⁶, Ch. Berger¹, G. Bernardi³⁰, R. Bernet³⁷, G. Bertrand-Coremans⁵, M. Besançon¹⁰, R. Beyer¹², P. Biddulph²³, P. Bispham²³, J.C. Bizot²⁸, V. Blobel¹⁴, K. Borrás⁹, F. Botterweck⁵, V. Boudry²⁹, A. Braemer¹⁵, W. Braunschweig¹, V. Brisson²⁸, D. Bruncko¹⁸, C. Brune¹⁶, R. Buchholz¹², L. Büngener¹⁴, J. Bürger¹², F.W. Büsler¹⁴, A. Buniatian^{12,39}, S. Burke¹⁹, M.J. Burton²³, G. Buschhorn²⁷, A.J. Campbell¹², T. Carli²⁷, F. Charles¹², M. Charlet¹², D. Clarke⁶, A.B. Clegg¹⁹, B. Clerbaux⁵, S. Cocks²⁰, J.G. Contreras⁹, C. Cormack²⁰, J.A. Coughlan⁶, A. Courau²⁸, M.-C. Cousinou²⁴, Ch. Coutures¹⁰, G. Cozzika¹⁰, L. Criegee¹², D.G. Cussans⁶, J. Cvach³¹, S. Dagoret³⁰, J.B. Dainton²⁰, W.D. Dau¹⁷, K. Daum³⁵, M. David¹⁰, C.L. Davis¹⁹, B. Delcourt²⁸, A. De Roeck¹², E.A. De Wolf⁵, M. Dirkmann⁹, P. Dixon¹⁹, P. Di Nezza³³, W. Dlugosz⁸, C. Dollfus³⁸, J.D. Dowell⁴, H.B. Dreis², A. Droutskoi²⁵, D. Düllmann¹⁴, O. Dünger¹⁴, H. Duhm¹³, J. Ebert³⁵, T.R. Ebert²⁰, G. Eckerlin¹², V. Efremenko²⁵, S. Egli³⁸, R. Eichler³⁷, F. Eisele¹⁵, E. Eisenhandler²¹, R.J. Ellison²³, E. Elsen¹², M. Erdmann¹⁵, W. Erdmann³⁷, E. Evrard⁵, A.B. Fahr¹⁴, L. Favart⁵, A. Fedotov²⁵, D. Feeken¹⁴, R. Felst¹², J. Feltse¹⁰, J. Ferencei¹⁸, F. Ferrarotto³³, K. Flamm¹², M. Fleischer⁹, M. Flieser²⁷, G. Flügge², A. Fomenko²⁶, B. Fominykh²⁵, M. Forbush⁸, J. Formánek³², J.M. Foster²³, G. Franke¹², E. Fretwurst¹³, E. Gabathuler²⁰, K. Gabathuler³⁴, F. Gaede²⁷, J. Garvey⁴, J. Gayler¹², M. Gebauer⁹, A. Gellrich¹², H. Genzel¹, R. Gerhards¹², A. Glazov³⁶, U. Goerlach¹², L. Goerlich⁷, N. Gogitidze²⁶, M. Goldberg³⁰, D. Goldner⁹, K. Golec-Biernat⁷, B. Gonzalez-Pineiro³⁰, I. Gorelov²⁵, C. Grab³⁷, H. Grässler², R. Grässler², T. Greenshaw²⁰, R. Griffiths²¹, G. Grindhammer²⁷, A. Gruber²⁷, C. Gruber¹⁷, J. Haack³⁶, D. Haidt¹², L. Hajduk⁷, M. Hampel¹, W.J. Haynes⁶, G. Heinzlmann¹⁴, R.C.W. Henderson¹⁹, H. Henschel³⁶, I. Herynek³¹, M.F. Hess²⁷, W. Hildesheim¹², K.H. Hiller³⁶, C.D. Hilton²³, J. Hladký³¹, K.C. Hoeger²³, M. Höppner⁹, D. Hoffmann¹², T. Holtom²⁰, R. Horisberger³⁴, V.L. Hudgson⁴, M. Hütte⁹, H. Hufnagel¹⁵, M. Ibbotson²³, H. Itterbeck¹, M.-A. Jabiol¹⁰, A. Jacholkowska²⁸, C. Jacobsson²², M. Jaffre²⁸, J. Janoth¹⁶, T. Jansen¹², L. Jönsson²², K. Johannsen¹⁴, D.P. Johnson⁵, L. Johnson¹⁹, H. Jung¹⁰, P.I.P. Kalmus²¹, M. Kander¹², D. Kant²¹, R. Kaschowitz², U. Kathage¹⁷, J. Katzy¹⁵, H.H. Kaufmann³⁶, O. Kaufmann¹⁵, S. Kazarian¹², I.R. Kenyon⁴, S. Kermiche²⁴, C. Keuker¹, C. Kiesling²⁷, M. Klein³⁶, C. Kleinwort¹², G. Knies¹², W. Ko⁸, T. Köhler¹, J.H. Köhne²⁷, H. Kolanoski³, F. Kole⁸, S.D. Kolya²³, V. Korbel¹², M. Korn⁹, P. Kostka³⁶, S.K. Kotelnikov²⁶, T. Krämerköpfer⁹, M.W. Krasny^{7,30}, H. Krehbiel¹², D. Krücker², U. Krüger¹², U. Krüner-Marquis¹², H. Küster²², M. Kühlen²⁷, T. Kurča³⁶, J. Kurzhöfer⁹, D. Lacour³⁰, B. Laforge¹⁰, F. Lamarche²⁹, R. Lander⁸, M.P.J. Landon²¹, W. Lange³⁶, U. Langenegger³⁷, J.-F. Laporte¹⁰, A. Lebedev²⁶, F. Lehner¹², C. Leverenz¹², S. Levonian²⁶, Ch. Ley², G. Lindström¹³, M. Lindstroem²², J. Link⁸, F. Linsel¹², J. Lipinski¹⁴, B. List¹², G. Lobo²⁸, P. Loch²⁸, H. Lohmander²², J.W. Lomas²³, G.C. Lopez¹³, V. Lubimov²⁵, D. Lüke^{9,12}, N. Magnussen³⁵, E. Malinovski²⁶, S. Mani⁸, R. Maraček¹⁸, P. Marage⁵, J. Marks²⁴, R. Marshall²³, J. Martens³⁵, G. Martin¹⁴, R. Martin²⁰, H.-U. Martyn¹, J. Martyniak⁷, S. Masson², T. Mavroidis²¹, S.J. Maxfield²⁰, S.J. McMahon²⁰, A. Mehta⁶, K. Meier¹⁶, T. Merz³⁶, A. Meyer¹⁴, A. Meyer¹², H. Meyer³⁵, J. Meyer¹², P.-O. Meyer², A. Migliori²⁹, S. Mikocki⁷, D. Milstead²⁰, J. Moeck²⁷, F. Moreau²⁹, J.V. Morris⁶, E. Mroczko⁷, D. Müller³⁸, G. Müller¹², K. Müller¹², P. Murin¹⁸, V. Nagovizin²⁵, R. Nahnhauser³⁶, B. Naroska¹⁴, Th. Naumann³⁶, P.R. Newman⁴, D. Newton¹⁹, D. Neyret³⁰, H.K. Nguyen³⁰, T.C. Nicholls⁴, F. Niebergall¹⁴, C. Niebuhr¹², Ch. Niedzballa¹, H. Niggli³⁷, R. Nisius¹, G. Nowak⁷, G.W. Noyes⁶, M. Nyberg-Werther²², M. Oakden²⁰, H. Oberlack²⁷, U. Obrock⁹, J.E. Olsson¹², D. Ozerov²⁵, P. Palmen², E. Panaro¹², A. Panitch⁵, C. Pascaud²⁸, G.D. Patel²⁰, H. Pawletta², E. Peppel³⁶, E. Perez¹⁰, J.P. Phillips²⁰, A. Pieuchot²⁴, D. Pitzl³⁷, G. Pope⁸, S. Prell¹², R. Prosi¹², K. Rabbert¹, G. Rädcl¹², F. Raupach¹, P. Reimer³¹, S. Reinshagen¹², H. Rick⁹, V. Riech¹³, J. Riedlberger³⁷, F. Riepenhausen², S. Riess¹⁴, M. Rietz², E. Rizvi²¹, S.M. Robertson⁴, P. Robmann³⁸, H.E. Roloff³⁶, R. Roosen⁵, K. Rosenbauer¹, A. Rostovtsev²⁵, F. Rouse⁸, C. Royon¹⁰, K. Rüter²⁷, S. Rusakov²⁶, K. Rybicki⁷, N. Sahlmann², D.P.C. Sankey⁶, P. Schacht²⁷, S. Schiek¹⁴, S. Schleich¹⁶, P. Schleper¹⁵, W. von Schlippe²¹, D. Schmidt³⁵, G. Schmidt¹⁴, A. Schöning¹², V. Schröder¹²,

E. Schuhmann²⁷, B. Schwab¹⁵, F. Sefkow¹², M. Seidel¹³, R. Sell¹², A. Semenov²⁵, V. Shekelyan¹², I. Sheviakov²⁶, L.N. Shtarkov²⁶, G. Siegmund¹⁷, U. Siewert¹⁷, Y. Sirois²⁹, I.O. Skillicorn¹¹, P. Smirnov²⁶, J.R. Smith⁸, V. Solochenko²⁵, Y. Soloviev²⁶, A. Specka²⁹, J. Spiekermann⁹, S. Spielman²⁹, H. Spitzer¹⁴, F. Squinabol²⁸, R. Starosta¹, M. Steenbock¹⁴, P. Steffen¹², R. Steinberg², H. Steiner^{12,40}, B. Stella³³, J. Stier¹², J. Stiewe¹⁶, U. Stöblein³⁶, K. Stolze³⁶, U. Straumann³⁸, W. Struczinski², J.P. Sutton⁴, S. Tapprogge¹⁶, M. Taševský³², V. Tchernyshov²⁵, S. Tchetchelnitski²⁵, J. Theissen², C. Thiebaux²⁹, G. Thompson²¹, P. Truöl³⁸, J. Turnau⁷, J. Tutas¹⁵, P. Uelkes², A. Usik²⁶, S. Valkár³², A. Valkárová³², C. Vallée²⁴, D. Vandenplas²⁹, P. Van Esch⁵, P. Van Mechelen⁵, Y. Vazdik²⁶, P. Verrecchia¹⁰, G. Villet¹⁰, K. Wacker⁹, A. Wagener², M. Wagener³⁴, A. Walther⁹, B. Waugh²³, G. Weber¹⁴, M. Weber¹², D. Wegener⁹, A. Wegner²⁷, T. Wengler¹⁵, M. Werner¹⁵, L.R. West⁴, T. Wilksen¹², S. Willard⁸, M. Winde³⁶, G.-G. Winter¹², C. Wittek¹⁴, E. Wünsch¹², J. Žáček³², D. Zarbock¹³, Z. Zhang²⁸, A. Zhokin²⁵, M. Zimmer¹², F. Zomer²⁸, J. Zsembory¹⁰, K. Zuber¹⁶, and M. zurNedden³⁸

¹ I. Physikalisches Institut der RWTH, Aachen, Germany^a

² III. Physikalisches Institut der RWTH, Aachen, Germany^a

³ Institut für Physik, Humboldt-Universität, Berlin, Germany^a

⁴ School of Physics and Space Research, University of Birmingham, Birmingham, UK^b

⁵ Inter-University Institute for High Energies ULB-VUB, Brussels; Universitaire Instelling Antwerpen, Wilrijk; Belgium^c

⁶ Rutherford Appleton Laboratory, Chilton, Didcot, UK^b

⁷ Institute for Nuclear Physics, Cracow, Poland^d

⁸ Physics Department and IIRPA, University of California, Davis, California, USA^e

⁹ Institut für Physik, Universität Dortmund, Dortmund, Germany^a

¹⁰ CEA, DSM/DAPNIA, CE-Saclay, Gif-sur-Yvette, France

¹¹ Department of Physics and Astronomy, University of Glasgow, Glasgow, UK^b

¹² DESY, Hamburg, Germany^a

¹³ I. Institut für Experimentalphysik, Universität Hamburg, Hamburg, Germany^a

¹⁴ II. Institut für Experimentalphysik, Universität Hamburg, Hamburg, Germany^a

¹⁵ Physikalisches Institut, Universität Heidelberg, Heidelberg, Germany^a

¹⁶ Institut für Hochenergiephysik, Universität Heidelberg, Heidelberg, Germany^a

¹⁷ Institut für Reine und Angewandte Kernphysik, Universität Kiel, Kiel, Germany^a

¹⁸ Institute of Experimental Physics, Slovak Academy of Sciences, Košice, Slovak Republic^f

¹⁹ School of Physics and Chemistry, University of Lancaster, Lancaster, UK^b

²⁰ Department of Physics, University of Liverpool, Liverpool, UK^b

²¹ Queen Mary and Westfield College, London, UK^b

²² Physics Department, University of Lund, Lund, Sweden^g

²³ Physics Department, University of Manchester, Manchester, UK^b

²⁴ CPPM, Université d'Aix-Marseille II, IN2P3-CNRS, Marseille, France

²⁵ Institute for Theoretical and Experimental Physics, Moscow, Russia

²⁶ Lebedev Physical Institute, Moscow, Russia^f

²⁷ Max-Planck-Institut für Physik, München, Germany^a

²⁸ LAL, Université de Paris-Sud, IN2P3-CNRS, Orsay, France

²⁹ LPNHE, Ecole Polytechnique, IN2P3-CNRS, Palaiseau, France

³⁰ LPNHE, Universités Paris VI and VII, IN2P3-CNRS, Paris, France

³¹ Institute of Physics, Czech Academy of Sciences, Praha, Czech Republic^{f,h}

³² Nuclear Center, Charles University, Praha, Czech Republic^{f,h}

³³ INFN Roma and Dipartimento di Fisica, Università "La Sapienza", Roma, Italy

³⁴ Paul Scherrer Institut, Villigen, Switzerland

³⁵ Fachbereich Physik, Bergische Universität Gesamthochschule Wuppertal, Wuppertal, Germany^a

³⁶ DESY, Institut für Hochenergiephysik, Zeuthen, Germany^a

³⁷ Institut für Teilchenphysik, ETH, Zürich, Switzerlandⁱ

³⁸ Physik-Institut der Universität Zürich, Zürich, Switzerlandⁱ

³⁹ Visitor from Yerevan Phys. Inst., Armenia

⁴⁰ On leave from LBL, Berkeley, USA

^a Supported by the Bundesministerium für Forschung und Technologie, FRG, under contract numbers 6AC17P, 6AC47P, 6DO57I, 6HH17P, 6HH27I, 6HD17I, 6HD27I, 6KI17P, 6MP17I, and 6WT87P

^b Supported by the UK Particle Physics and Astronomy Research Council, and formerly by the UK Science and Engineering Research Council

^c Supported by FNRS-NFWO, IISN-IKW

^d Supported by the Polish State Committee for Scientific Research, grant nos. 115/E-743/SPUB/P03/109/95 and 2 P03B 244 08p01, and Stiftung für Deutsch-Polnische Zusammenarbeit, project no.506/92

^e Supported in part by USDOE grant DE F603 91ER40674

^f Supported by the Deutsche Forschungsgemeinschaft

^g Supported by the Swedish Natural Science Research Council

^h Supported by GA ČR, grant no. 202/93/2423, GA AV ČR, grant no. 19095 and GA UK, grant no.

342

ⁱ Supported by the Swiss National Science Foundation

1 Introduction

In high energy physics, the parton model together with the theory of strong interaction, Quantum-Chromo-Dynamics (QCD), have been shown to provide a good description of a variety of different processes involving hadrons in the final and/or initial state (e.g. in e^+e^- collisions[1], in hadron-hadron collisions[2] and in lepton-hadron scattering[3]). However, so far QCD has not been able to make predictions, derived from first principles, for a class of hadron-hadron collisions known as diffractive scattering. This class is characterised experimentally as peripheral collisions between the incoming hadrons, whereby the scattered hadrons keep their original identity or break up dominantly into a system of low invariant mass. This generally leads to experimentally observable large rapidity gaps in these collisions. Regge theory applied to hadronic interactions models diffractive collisions[4] as the exchange of an object called the pomeron (IP), which carries only the quantum numbers of the vacuum and thus no colour charge. Attempts have been made to study the nature of diffractive exchange, and it has been suggested that the pomeron has partonic structure[5], indications for which were found in proton-antiproton collisions by the UA8 experiment[6].

At the turn-on of the electron-proton (ep) collider HERA, at DESY, Hamburg, a class of deep-inelastic scattering (DIS) events was observed which exhibited in the hadronic final state an unusually large rapidity gap (LRG) with almost no hadronic energy flow around the direction of the proton remnant[7, 8]. Recent cross-section measurements[9, 10] have shown that these events exhibit characteristics similar to those of diffractive hadronic collisions. At low Bjorken- x (see below for kinematic definitions) the diffractive contribution to the total DIS cross-section, and thus to the proton structure function F_2 , has been quantified in the form of a diffractive structure function $F_2^{D(3)}$ [9, 10]. The dependence of $F_2^{D(3)}$ on the appropriate deep-inelastic kinematic variables x_P , Q^2 , and β (see below) has been measured. It demonstrates both that the diffractive deep-inelastic ep process can be interpreted as deep-inelastic scattering of the incident electron off a colourless object coupling to the proton in the diffractive ep interaction, and that the structure of this object is consistent with being of a partonic nature. Thus deep-inelastic scattering may be pictured as in figure 1 (a), and the diffractive contri-

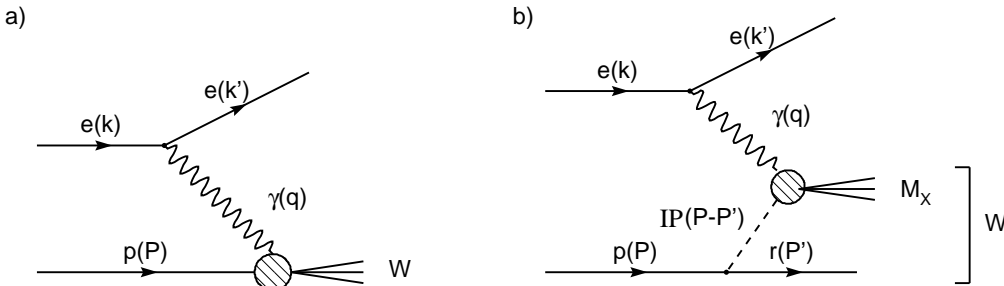


Figure 1: Schematic picture for deep-inelastic scattering: non-diffractive (a) and diffractive (b).

bution to it as in figure 1 (b), where the process is considered in the phenomenology which is used to quantify diffractive interactions in high energy hadron-hadron physics. In each case a virtual photon (in the kinematic region investigated, contributions from Z^0 exchange can be neglected) probes a hadronic object. For non-diffractive DIS this object is a proton, whereas in the diffractive case this is taken to be a colour neutral object emitted from the proton. The proton remnant system in the latter case remains colourless and thus a gap in rapidity is produced. Note that experimentally we observe events which have a rapidity gap, as defined below. Throughout this paper we will however use the terms “diffractive” event and “LRG event” synonymously.

Using the four-momenta k of the incident electron, q of the virtual photon and P of the incident proton the following kinematical variables can be defined:

$$Q^2 = -q^2, \quad x = \frac{Q^2}{2P \cdot q}, \quad y = \frac{P \cdot q}{P \cdot k} \quad \text{and} \quad W^2 = (P + q)^2, \quad (1)$$

where Q^2 is the squared virtuality of the photon and x is the Bjorken scaling variable, which in the naïve Quark-Parton Model (QPM) can be interpreted as the fraction of the proton's momentum carried by the struck quark. In the rest frame of the proton y is the fraction of the electron energy transferred to the proton. W is the invariant mass of the photon-proton system and is equal to the invariant mass of the total final state excluding the scattered electron.

Additional kinematical variables can be defined using the four-momentum P' of the colourless remnant (either a nucleon or a higher mass baryon excitation) in the final state:

$$x_{\mathcal{P}} = \frac{q \cdot (P - P')}{q \cdot P}, \quad \beta = \frac{Q^2}{2q \cdot (P - P')} \quad \text{and} \quad t = (P - P')^2. \quad (2)$$

The variables x , $x_{\mathcal{P}}$ and β are related via $x = x_{\mathcal{P}}\beta$. Defining M_X to be the invariant mass of the virtual photon-pomeron system (i.e the invariant mass of that part of the final state not associated with the colourless remnant and separated from the latter by a LRG), $x_{\mathcal{P}}$ and β can be written as

$$x_{\mathcal{P}} = \frac{Q^2 + M_X^2 - t}{Q^2 + W^2 - M_p^2} \quad \text{and} \quad \beta = \frac{Q^2}{Q^2 + M_X^2 - t}, \quad (3)$$

where M_p is the mass of the proton. When M_p^2 and $|t|$ are small ($M_p^2 \ll Q^2$ and $\ll W^2$ and $|t| \ll Q^2$ and $\ll M_X^2$), $x_{\mathcal{P}}$ can be interpreted as the fraction of the proton's four-momentum transferred to the pomeron, and β can be viewed as the fraction of the pomeron's four-momentum carried by the quark entering the hard scattering. In the kinematic region under investigation both M_p^2 and $|t|$ can be neglected and therefore $x_{\mathcal{P}}$ and β can be calculated from M_X^2 , Q^2 and W^2 as

$$x_{\mathcal{P}} \approx \frac{M_X^2 + Q^2}{W^2 + Q^2} \quad \text{and} \quad \beta \approx \frac{Q^2}{M_X^2 + Q^2}. \quad (4)$$

The consistency of the dependence of $F_2^{D(3)}$ on β and Q^2 with a partonic interpretation of the pomeron[9, 10] implies that the hadronic final state in deep-inelastic diffractive scattering is expected to show evidence for parton production and effects of perturbative QCD of a nature similar to deep-inelastic ep scattering at appropriate ($x \sim \beta$) Bjorken- x . This picture can be further tested through detailed measurements of the hadronic final state. In this paper we present an analysis of the hadronic final states for diffractive and non-diffractive DIS, and compare the results with QCD inspired models. The analysis concentrates on the observed energy flow in the laboratory frame relative to the expected direction of the struck quark. In the naïve Quark-Parton Model this direction can be calculated from the measurement of the scattered electron using four-momentum conservation. Such prediction of the quark direction is not possible in e^+e^- and hadron-hadron collisions. There the measured hadronic final state must itself be used, e.g. by defining jet directions which then can be related to parton directions. In[11] the ZEUS collaboration compared the final state of events with a LRG to that of events without a gap using energy flow measurements and concluded that in DIS with a LRG QCD radiation is strongly suppressed. Recently a comparison of charged particle spectra for the two classes of events was performed by the ZEUS collaboration[12], where they observed similarities between DIS with a LRG at HERA and DIS at lower W ($\approx M_X$).

In this analysis, properties of the observed energy flow are defined which are sensitive to effects of perturbative QCD. The evolution of these properties with the kinematical variables is investigated. The data presented are corrected for detector effects. From the diagrams shown in figure 1 it is expected that

the different kinematics in the two cases imply differences in the available phase space for QCD effects in the hadronic final state. The invariant mass of the system built from the photon and the probed object is given by W for non-diffractive DIS and M_X in the diffractive case, where $M_X \ll W$. The relevance of this scale for hadron production in the diffractive process will be tested by considering DIS at a reduced proton beam energy. This feature is also a key ingredient of several more sophisticated models for diffractive DIS, such as RAPGAP[13]. Here it is assumed that the hard scattering occurs off a partonic constituent of a pomeron emitted from the proton as shown in diagram 1 (b). QCD effects of parton showers and hadronization are included in this model. However, alternative explanations for the diffractive process exist. The two models LEPTO[14] and HERWIG[15], originally developed for non-diffractive DIS, in the most recent versions also generate events with a leading colourless remnant. These models do not involve explicitly the emission of a pomeron but instead produce the gap through non-perturbative QCD effects in the evolution of the final state produced by deep-inelastic scattering of a partonic constituent of the proton. The predictions of these models will be compared with the data.

The paper is organized as follows. After a short description of the H1 detector (section 2), the data taking and the event selection are briefly discussed (section 3). Then are described the models of the hadronic final state used in deep-inelastic scattering (section 4), the procedure to correct for detector effects, and the sources of systematic errors (section 5). In section 6 the characteristic properties of the energy flow are explained and the estimators used are defined. Results and the comparison with different model predictions are presented in section 7. The paper is summarized in section 8. In an appendix the measured values of the estimators are listed together with their statistical and systematic errors.

2 The H1 Detector

The general layout of the H1 detector (described in more detail in [16]) is as follows: the interaction region is surrounded with tracking devices which measure the momenta of charged particles and reconstruct the position of the interaction point. These tracking detectors are enclosed by a calorimetric region which allows the measurement of the energy and the direction of charged and neutral particles. All these detectors are situated within a magnetic field of 1.15 T, generated by a superconducting coil. The flux return yoke of this coil is instrumented to identify muons and to measure energy escaping the main calorimeters. In the following the components of the H1 detector of particular relevance to this analysis are briefly presented. In the coordinate system used, the proton beam direction defines the $+z$ -axis. The region of polar angle $0 < \theta < \pi/2$ is called “forward region” and corresponds to positive values of pseudo-rapidity $\eta = -\ln \tan \frac{\theta}{2}$, whereas $\eta < 0$ in the “backward region” ($\pi/2 < \theta < \pi$).

The measurement of charged particle tracks and the determination of the interaction point is made with a system of interleaved drift and multiwire proportional chambers covering the central and forward regions of the detector ($7^\circ < \theta < 165^\circ$ corresponding to $-2.0 < \eta < 2.8$) over the full azimuthal range. The backward region is equipped with a proportional chamber (BPC) measuring charged particle positions in the angular range $155^\circ < \theta < 174.5^\circ$ in front of the backward calorimeter (BEMC).

The main calorimeter is a fine-grained liquid argon (LAr) calorimeter[17], covering a range in polar angle from 4° to 155° ($-1.51 < \eta < 3.35$). It consists of an electromagnetic section with lead absorbers ($20 - 30 X_0$) and a hadronic part with steel absorbers, giving a total interaction length of $5 - 8 \lambda$. The energy resolution as measured in test beams[18] is $\sigma/E \approx 12\%/\sqrt{E}$ for electrons and $\approx 50\%/\sqrt{E}$ for hadrons, with E in GeV. The energy scale is known to about 2% for electrons and to about 5% for hadrons.

Covering the η range -3.35 to -1.35 ($151^\circ < \theta < 176^\circ$), the backward electromagnetic calorimeter (BEMC) allows the measurement of the scattered electron for low Q^2 DIS events ($5 \text{ GeV}^2 < Q^2 <$

100 GeV²) and provides information on hadrons scattered in this region. The BEMC is a lead–scintillator sandwich calorimeter (22.5 X_0 or 1 hadronic absorption length), with a resolution of $\approx 10\%/\sqrt{E}$ for electrons and an uncertainty in the energy scale for electrons of about 1.7%. Located behind the calorimeter is a time–of–flight system, consisting of scintillators which veto upstream interactions of the proton beam.

The very forward region is equipped with a copper–silicon calorimeter (PLUG), covering a range in η from 3.54 to 5.08. The longitudinal thickness is 4.25 hadronic absorption lengths. A muon spectrometer surrounds the beam pipe outside the flux return yoke in the forward direction. It consists of a toroidal magnet sandwiched between two sets of drift chambers and is used to detect charged particles from ep interactions in the range $5.0 < \eta < 6.6$ by means of secondary particles which they produce from interactions in the beam pipe and adjunct material. The latter two detectors are used in this analysis to tag particle production in the forward region close to the proton beam direction.

For the determination of the luminosity the process $ep \rightarrow ep\gamma$ is used, where the electrons and photons are measured in two calorimeters located far downstream of the detector in the electron beam direction (the electron “tagger” at $z = -33$ m and the photon “tagger” at $z = -102$ m).

3 Data Taking and Event Selection

In 1993 the HERA collider operated with a 26.7 GeV electron beam and an 820 GeV proton beam, giving a centre of mass energy of $\sqrt{s} = 296$ GeV. The data used for this analysis correspond to an integrated luminosity of 294 nb⁻¹. The events used here were triggered by requiring a cluster with an energy larger than 4 GeV in the BEMC and no veto from the time–of–flight system. This trigger has an efficiency of 99% for events containing an electron with an energy of more than 10 GeV in the angular acceptance of the BEMC and provides a sample of DIS events at low Q^2 ($5 \text{ GeV}^2 < Q^2 < 100 \text{ GeV}^2$).

The measurement of the energy E'_e and the polar angle θ_e of the scattered electron is used to determine the kinematical variables $Q^2 = 4E_e E'_e \cos^2(\theta_e/2)$ and $y = 1 - (E'_e/E_e) \sin^2(\theta_e/2)$, where E_e is the electron beam energy. Bjorken x and the square of the invariant mass of the total hadronic system, W^2 , can be calculated from Q^2 and y using the relations $x = Q^2/(ys)$ and $W^2 = sy - Q^2$.

The selection of deep–inelastic scattering events follows closely that used in the recent measurement of the deep–inelastic structure function $F_2(x, Q^2)$ [19] and the diffractive structure function $F_2^{D(3)}(x, Q^2, x_P)$ [9] by H1. The main requirements are an electron candidate in the backward calorimeter, a reconstructed interaction point, and a minimal invariant mass of the hadronic final state:

- The electron candidate is required to have an energy $E'_e > 10.6$ GeV and to be found within the angular acceptance of the BEMC: $155^\circ < \theta_e < 173^\circ$. In addition, electron identification cuts to suppress background from photoproduction events are made using the information obtained from the cluster radius and the matching of the cluster with a charged particle signal in the BPC.
- A reconstructed vertex close to the nominal interaction point is demanded: $|z_{vertex} - z_{vertex}^{nominal}| < 30$ cm.
- To ensure accurate reconstruction of the kinematics from the detected scattered electron, $y > 0.05$ is required since the reconstruction deteriorates at low values of y .

The selected events cover the kinematical range $10^{-4} < x < 10^{-2}$ and $7.5 \text{ GeV}^2 < Q^2 < 100 \text{ GeV}^2$ with an average value for W^2 of 23000 GeV² ($4300 \text{ GeV}^2 < W^2 < 53000 \text{ GeV}^2$).

For the measurement of energy flow and the invariant mass of the final state, clusters reconstructed in the LAr calorimeter and in the BEMC were used. In the BEMC, only clusters with an energy larger than 400 MeV are considered.

The sample of DIS events obtained contains events with and without a large gap in rapidity. DIS events without a gap are selected by demanding

- a minimal energy deposit in the forward region measured in the LAr calorimeter: $E_{forward} > 0.5$ GeV (as used in [20, 21]), where $E_{forward}$ is the summed energy in the the region $4.4^\circ < \theta < 15^\circ$, corresponding to $2.03 < \eta < 3.26$.

This requirement together with the DIS selection described above results in 15242 events. The only significant background to these events from other ep interactions is due to photoproduction which contributes about 9% of the events at the lowest value of $x \approx 2 \cdot 10^{-4}$ and can be ignored for values of $x > 4 \cdot 10^{-4}$.

For the selection of DIS events with a large rapidity gap, as described in detail in [9], the existence of a region around the proton remnant direction with almost no hadronic energy flow is required. The detector components used for this selection give access to the very forward region (up to a pseudo-rapidity of $\eta \approx 6.6$):

- The energy deposited in the Plug calorimeter has to be smaller than 1 GeV and the number of reconstructed hit pairs in the forward muon spectrometer has to be smaller than 2. In addition $\eta_{max,LAr} < 3.2$ is required, where $\eta_{max,LAr}$ is the maximum pseudo-rapidity of all clusters in the LAr calorimeter with $E > 0.4$ GeV.

Applying these cuts together with the DIS kinematical cuts leads to a sample of 1721 events with a LRG. This sample consists of events where a leading hadron or cluster of hadrons R_c in the forward direction escapes detection by remaining in the beam pipe. The acceptance in the invariant mass M_R of R_c is specified by the forward detectors used to define the sample. As M_R increases from the mass of the proton to 4 GeV the acceptance decreases from 100% to less than 5%; above 4 GeV the acceptance is always less than 5%. In the central detector the remainder of the final state, separated by a gap from R_c , is detected. The invariant mass M_X of this system defines through equation 4 the kinematic variable $x_{\mathcal{P}}$ for each event. The data sample¹ used covers the range $2 \cdot 10^{-4} < x_{\mathcal{P}} < 2 \cdot 10^{-2}$. In all results presented, diffractive DIS is taken to be for $x < x_{\mathcal{P}} < 0.02$.

4 Monte Carlo Models for the Hadronic Final State

The Monte Carlo models for DIS can be separated into three parts. The hard interaction of a virtual boson with a parton is simulated using the leading order electroweak cross-section for parton scattering including the first order QCD correction given by the exact $O(\alpha_S)$ matrix elements (these are: the Born term for boson-quark scattering, hard gluon Bremsstrahlung, and the boson-gluon fusion process). A parton cascade includes higher order QCD corrections to generate additional partons. The resulting coloured partons hadronize to give the observable particles.

The models differ mainly in the details of the parton cascade and the phenomenological description of the hadronization. The following description of the models emphasizes these different approaches.

¹The sample of events with a gap and that without a gap are not completely disjoint. About 5% of events without a gap are also classified as events with a gap. This however does not effect the conclusions drawn.

LEPTO [14] uses the the leading–log approximation based on the Altarelli–Parisi evolution equations [22] for the parton showers. The fragmentation is done via the Lund string model[23] as implemented in JETSET[24].

The new version (6.3) of LEPTO differs from the previous version (6.1) mainly in two aspects. Firstly, the treatment of scattering involving a sea–quark has been modified, motivated by the poor description of the measured transverse energy flow in the forward region[21] given by version 6.1. Secondly, the possibility of colour rearrangement in the final state through soft gluon exchange with negligible change in the momenta of the partons has been introduced, allowing the generation of events with a leading colourless remnant. This soft colour interaction[25] is a non–perturbative interaction of the coloured quarks and gluons with the colour medium of the proton. This way of generating a colour–neutral subsystem is similar to the ideas of Buchmueller and Hebecker[26], who performed a calculation of the diffractive cross–section on the parton level. The size of the diffractive contribution is determined by a probability² that such a colour exchange occurs between two colour charges, leading for part of the cross–section to the formation of colour singlet subsystems separated in rapidity.

ARIADNE [27] is a generator for QCD cascades only. In this analysis, two versions (4.03 and 4.07) are used. The former version is used to calculate the correction for detector effects for events without a gap (see next section). Previous analyses[21, 28] have shown that this version gives a reasonable description of the data. The version 4.07 is used in comparison with non–diffractive DIS. For the modelling of the electroweak interaction the corresponding parts of LEPTO[14] are used. Gluon radiation is performed in ARIADNE by an implementation of the Colour Dipole Model[29]. In this model, gluon emission from a quark–antiquark pair is treated as radiation from a colour dipole formed by this pair. In contrast to the quarks in e^+e^- –annihilation, the proton remnant in DIS is assumed to be extended. This leads to a suppression of the phase space for gluon radiation. In version 4.07 the struck quark is considered to be extended as well. The latter modification was motivated by the disagreement between HERA data and the ARIADNE (version 4.03) prediction in the region of the struck quark[21, 28]. The hadronization is done using the Lund string model (JETSET). In version 4.07 diffractive DIS is modelled via the emission of a pomeron from the proton and subsequent hard scattering on a partonic constituent of the pomeron. This mechanism follows the spirit of RAPGAP (see below) and is not investigated in this paper. In[30] Lönnblad demonstrates that in the framework of the Colour Dipole Model colour reconnections cannot reproduce the diffractive contribution to DIS in contrast to the LEPTO model.

HERWIG [15] is a general purpose generator for high energy hadronic processes. The parton shower algorithm (in the leading logarithmic approximation) takes into account colour coherence as well as soft gluon interference. The hadronization in HERWIG is performed using the concept of cluster fragmentation, where gluons are split non–perturbatively into quark–antiquark pairs. The latter are combined into colour singlet clusters, which are split further until a minimum value of the cluster mass is reached. In the most recent version (5.8d)[31], as used in this analysis, HERWIG can generate a diffractive contribution to DIS, the size of which is sensitive to a parameter³ determining the mass distribution for the cluster splitting in the hadronization.

For all the above models the MRS(H)[32] set of parton distributions for the proton was used. These were determined using data from various experiments including the F_2 measurements from HERA made

²The default value for PARL(7) is 0.2, this leads to a diffractive contribution of about 7% to the deep–inelastic cross section in the kinematic range considered. A variation of this parameter between 0.1 and 0.5 gives a change in this fraction between 5% and 9% but no significant changes in the measured energy flow are observed within the two event classes.

³The chosen value for PSPLT is 0.7, this leads to a diffractive contribution of 6%. A variation of this parameter between 0.5 and 1.0 gives contributions of 2% and 8%. However the change in PSPLT results in significant changes in the predicted energy flow properties for both classes of events in contrast to LEPTO.

in 1992[33, 34]. In addition to the kinematical selection as described above a cut on the summed energy $E_{forward}$ of all particles produced in the range $2.03 < \eta < 3.26$ is performed by demanding $E_{forward} > 0.5$ GeV for the distributions obtained from the models in the non-diffractive case.

It should be stressed that the LEPTO model as well as the HERWIG model in the most recent versions can generate a diffractive contribution to the DIS cross-section compatible with the measurement without explicitly involving the concept of deep-inelastic electron-pomeron scattering. These events are selected by demanding that $\eta_{max}^{gen} < 3.2$, where η_{max}^{gen} is the maximum pseudo-rapidity of all particles with $E > 0.4$ GeV and $\eta < 6.6$. Both models broadly reproduce the x_P dependence of $F_2^{D(3)}$ as measured in[9] and thus the one of the deep-inelastic diffractive cross-section. Most of the parameters in these models which influence the description of the hadronic final state are restricted by measurements of non-diffractive DIS, leaving at present only a few parameters free for the modelling of diffractive DIS. Events with a LRG also occur in the previous versions of the models but at a very small rate (being due to extreme fluctuations in the fragmentation).

RAPGAP [13] models diffractive DIS by the emission of a pomeron from the proton, described by a flux factor depending only on x_P and t . The pomeron is taken to be an object with a partonic structure described by parton densities, which depend on β and Q^2 . This hypothesis is consistent with the recent measurements of the diffractive structure function $F_2^{D(3)}$ [9, 10]. In the version used (1.3) the parton content of the pomeron can be chosen to be either a quark-antiquark pair or two gluons. Within this analysis, the parton densities $p(z)$ are chosen to be “hard” distributions ($[z \cdot p(z)] \sim z \cdot (1 - z)$), where z is the fraction of the momentum of the parton relative to the pomeron. A soft parton density ($[z \cdot p(z)] \sim (1 - z)^5$) is excluded by the measurement of $F_2^{D(3)}$ as described in [9]. A mixture of “hard quark” and “hard gluon” densities was used such that an equal number of events are generated for both densities in the kinematic range considered. This leads to a sample in which, for $\beta \leq 0.1$, more than 70% (and for $\beta \geq 0.9$ less than 5%) of the events are of the “hard gluon” type. The mixture has been chosen to get a good description of the measured diffractive structure function $F_2^{D(3)}$ and was found to be able to describe the measured energy flow. Additional partons due to QCD radiation are generated using the Colour Dipole model, the subsequent hadronization is performed with JETSET. The version of RAPGAP used does not include the evolution of parton densities with Q^2 .

5 Correction for Detector Effects

The correction of the measured energy flow for detector effects in non-diffractive DIS is done using events generated with the ARIADNE 4.03[27] model, which have been passed through a simulation of the H1 detector response. They are reconstructed in the same way as is done for the data. For diffractive DIS the same procedure is applied using the RAPGAP 1.3[13] model.

For each distribution shown, a set of bin-by-bin correction factors is calculated by forming the ratio of the bin-contents for the generated events (at the particle level) to the corresponding bin-contents for the reconstructed events (from the detector simulation, i.e. at the detector level). To obtain the corrected value, the raw data bin-contents have to be multiplied by the correction factor. The derived factors vary only moderately from bin to bin and have values typically between 0.8 and 1.2.

In the determination of the systematic error associated with the correction factors, the following effects were considered:

- Variation of the energy scale for the scattered electron in the BEMC. The energy scale is known to $\pm 1.7\%$.

- Uncertainty in the polar angle of the scattered electron. An error of ± 2 mrad was taken into account.
- Uncertainty in the hadronic energy scale in the LAr calorimeter. From studies using p_T -balance between the scattered electron and the hadronic final state, the energy scale is known to an accuracy of $\pm 5\%$.
- Uncertainty in the hadronic energy scale in the BEMC. The hadronic energy scale in the BEMC was assumed to be known to $\pm 20\%$.
- Dependence on the model used for corrections. For events without a LRG, a comparison between the correction factors obtained using the ARIADNE and the LEPTO model was performed. In the case of DIS with a LRG, the RAPGAP model assuming either a quark parton density or a gluon density alone was studied.
- The effect of initial state photon radiation off the electron has been estimated with the DJANGO model[35].
- The effect of background from photoproduction ($Q^2 \approx 0$) has been investigated using H1 photoproduction data in which the scattered electron is detected in the electron calorimeter of the luminosity system and an electron candidate is found in the BEMC. The values of the estimators obtained were found to be smaller than those in the DIS data. Using a value of 9% for the contamination from photoproduction at the lowest value of $x \approx 2 \cdot 10^{-4}$ [19] (contamination negligible for $x > 3 \cdot 10^{-4}$) an asymmetric contribution to the systematic error is obtained.

All contributions have been added quadratically to give a value of the systematic error for each bin considered. The error bars shown contain the statistical error (inner bars) as well as the total error (full error bar) which has been obtained by adding statistical and systematic errors in quadrature.

6 Characteristic Properties of the Energy Flow

Within the framework of the naïve Quark-Parton Model, the measurement of the four-momentum of the scattered electron determines the direction of the quark struck in the deep-inelastic scattering. Using conservation of four-momentum and assuming that the partons are massless and the proton remnant has negligible transverse momentum, the polar angle of the struck quark can be calculated from the energy and the polar angle of the scattered electron. The pseudo-rapidity η_q of the struck quark can be expressed in terms of the kinematical variables x and Q^2 as:

$$\eta_q = \frac{1}{2} \ln \left[x \left(\frac{xs}{Q^2} - 1 \right) \frac{E_p}{E_e} \right] \quad (5)$$

where $E_p(E_e)$ is the proton (electron) beam energy and s is the square of the centre of mass energy. The scattered electron and the struck quark are (in the QPM) back-to-back in azimuth, i.e. :

$$\phi_q = \phi_e + \pi \quad (6)$$

To look at deviations from these expectations, the following two variables are used:

$$\Delta\eta = \eta - \eta_q \quad (7)$$

$$\Delta\phi = \phi - \phi_q \quad (8)$$

where η (ϕ) denotes the pseudo-rapidity (azimuthal angle) of a particle or calorimetric cluster.

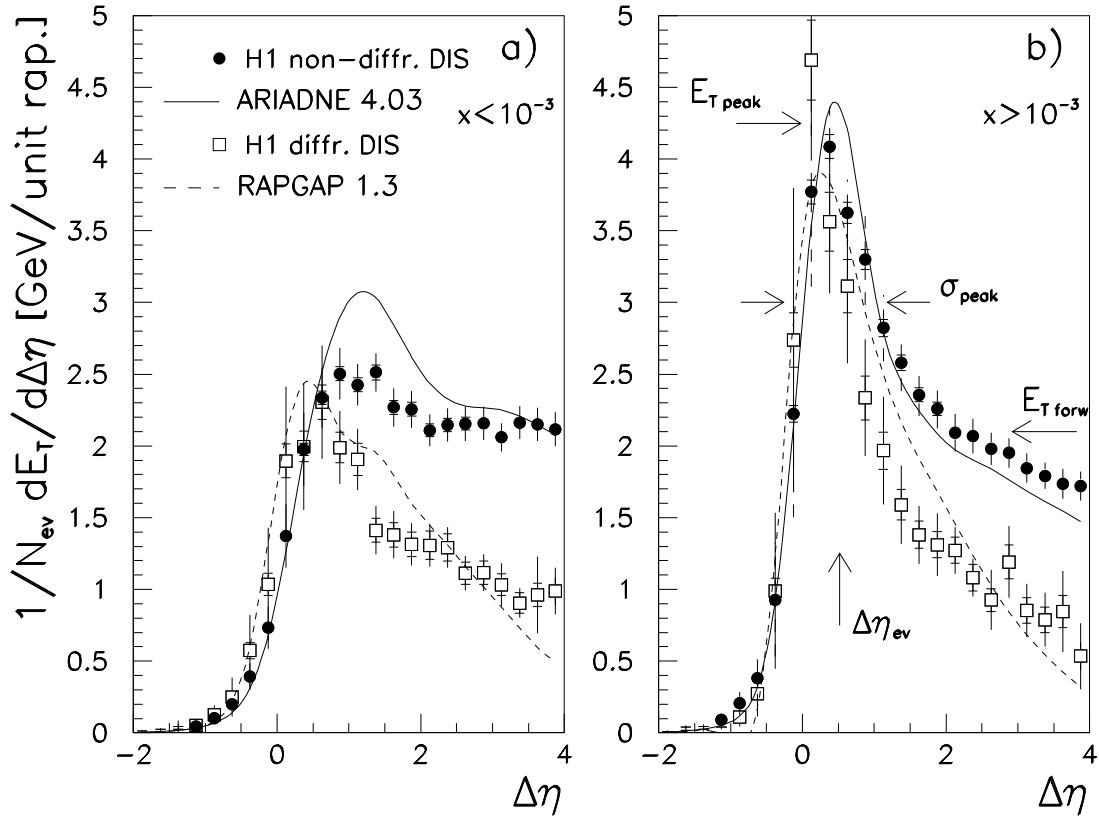


Figure 2: Measured transverse energy flow relative to the calculated struck quark direction. Shown are non-diffractive (“non-diffr. DIS”) and diffractive (“diffr. DIS”) data, both corrected for detector effects. Also indicated are the models for DIS (ARIADNE) and for diffractive DIS (RAPGAP), which have been used to do the correction. Data with $x < 10^{-3}$ are shown in (a), those with $x > 10^{-3}$ in (b). In both figures the proton direction corresponds to large positive values of $\Delta\eta$. In (b) the meaning of the 4 estimators for the energy flow is also indicated using the non-diffractive data.

The measured transverse energy flow $\frac{dE_T}{d\Delta\eta}$ (integrated over azimuthal angle) around the expected naïve QPM direction ($\Delta\eta = 0$) is shown in figure 2. Displayed are the energy flows for non-diffractive as well as for diffractive DIS, in two regions of x ($x < 10^{-3}$ and $x > 10^{-3}$). The measured transverse energy flow relative to the naïve QPM prediction can be separated into that around $\Delta\eta = 0$ (this will be denoted the “current region” in the following) and the remainder of the energy flow at positive values of $\Delta\eta$ towards the direction of the proton remnant (the “forward region”). The properties of the energy flow depend strongly on the kinematics, as may be seen in figure 2. The maximum of the transverse energy in the current region is shifted to positive values of $\Delta\eta$ for all DIS data. The measured shape of the energy flows for the diffractive and the non-diffractive case is found to be very similar in the current region, whereas in the forward region a reduced amount of transverse energy is expected for diffractive ep DIS with a leading colourless remnant compared to the non-diffractive process. Also shown are the two models used to correct for detector effects, ARIADNE (version 4.03) for non-diffractive and RAPGAP (version 1.3) for diffractive DIS.

To investigate in more detail the dependence of the hadronic final state on kinematical variables and to discuss the observed similarities as well as the differences for the two cases, 4 estimators of characteristic properties of the measured transverse energy flow are defined as illustrated qualitatively in figure 2 (b). These estimators are calculated for each event using the measured calorimetric clusters and correction factors in case of the data and stable particles in the case of the model calculations.

Firstly, the deviation $\Delta\eta_{ev}$ in pseudo-rapidity of the maximum in transverse energy from the expected naïve QPM direction is determined. Secondly the magnitude E_{Tpeak} of the energy flow at this position is calculated. Next the width σ_{peak} in pseudo-rapidity of the energy flow around the maximum is quantified. Finally the level of transverse energy E_{Tforw} away from the current region towards the direction of the proton remnant is determined.

$\Delta\eta_{ev}$ is calculated as an E_T -weighted average of $\Delta\eta$ in the region with $|\Delta\eta| < 2$ around the expected quark direction, restricting the range in $\Delta\phi$ to values with $|\Delta\phi| < 1.5$:

$$\Delta\eta_{ev} = \frac{\sum_{|\Delta\eta|<2,|\Delta\phi|<1.5} E_T \Delta\eta}{\sum_{|\Delta\eta|<2,|\Delta\phi|<1.5} E_T} \quad (9)$$

Having calculated the observed deviation for an event, the magnitude E_{Tpeak} in transverse energy at this position (normalized to one unit of pseudo-rapidity) is determined by adding up the transverse energy in a region of ± 0.25 in pseudo-rapidity:

$$E_{Tpeak} = \frac{1}{0.5} \sum_{|\Delta\eta - \Delta\eta_{ev}| < 0.25} E_T \quad (10)$$

The width σ_{peak} in pseudo-rapidity of the energy flow in the current region is obtained by determining the r.m.s of the $\Delta\eta$ distribution weighted with E_T around the measured position $\Delta\eta_{ev}$ of the maximum in a $\Delta\eta$ range of ± 1 :

$$\sigma_{peak} = \sqrt{\frac{\sum_{|\Delta\eta - \Delta\eta_{ev}| < 1} E_T \cdot (\Delta\eta - \Delta\eta_{ev})^2}{\sum_{|\Delta\eta - \Delta\eta_{ev}| < 1} E_T}} \quad (11)$$

E_{Tforw} (normalized to one unit of pseudo-rapidity) is determined in the region starting one unit of pseudo-rapidity forward of the measured position of the maximum E_T in the current region ($\eta_q + \Delta\eta_{ev}$) up to a fixed value of pseudo-rapidity ($\eta = 3$) – to stay away from the acceptance limit of the LAr calorimeter.

$$E_{Tforw} = \frac{1}{3 - (\eta_q + \Delta\eta_{ev} + 1)} \sum_{(\eta_q + \Delta\eta_{ev} + 1) < \eta < 3} E_T \quad (12)$$

7 Results

In this section, the dependence of the measured transverse energy flow on kinematical variables is studied for diffractive and non-diffractive DIS, using the 4 estimators defined in the previous section. First the x dependence of the estimators for diffractive and non-diffractive data is compared. Next, the non-diffractive measurements are confronted with the most recent versions of models for DIS. The characteristics of the hadronic final state in diffractive DIS are then investigated for evidence of significant discrepancy from the expectation given by a partonic process with the related effects of perturbative QCD. To this end, first a phenomenological model of ep DIS in the same kinematic region is investigated, and then the diffractive final state is compared with a set of different models of deep-inelastic ep diffraction.

Figure 3 shows the dependence of the estimators on x for diffractive and non-diffractive DIS. The measured values, together with the statistical and systematic errors, can be found in the appendix in tables 1 and 2. For both cases a significant deviation $\Delta\eta_{ev}$ of the maximum in transverse energy from the naïve QPM expectation is observed which strongly increases with decreasing values of x . For diffractive

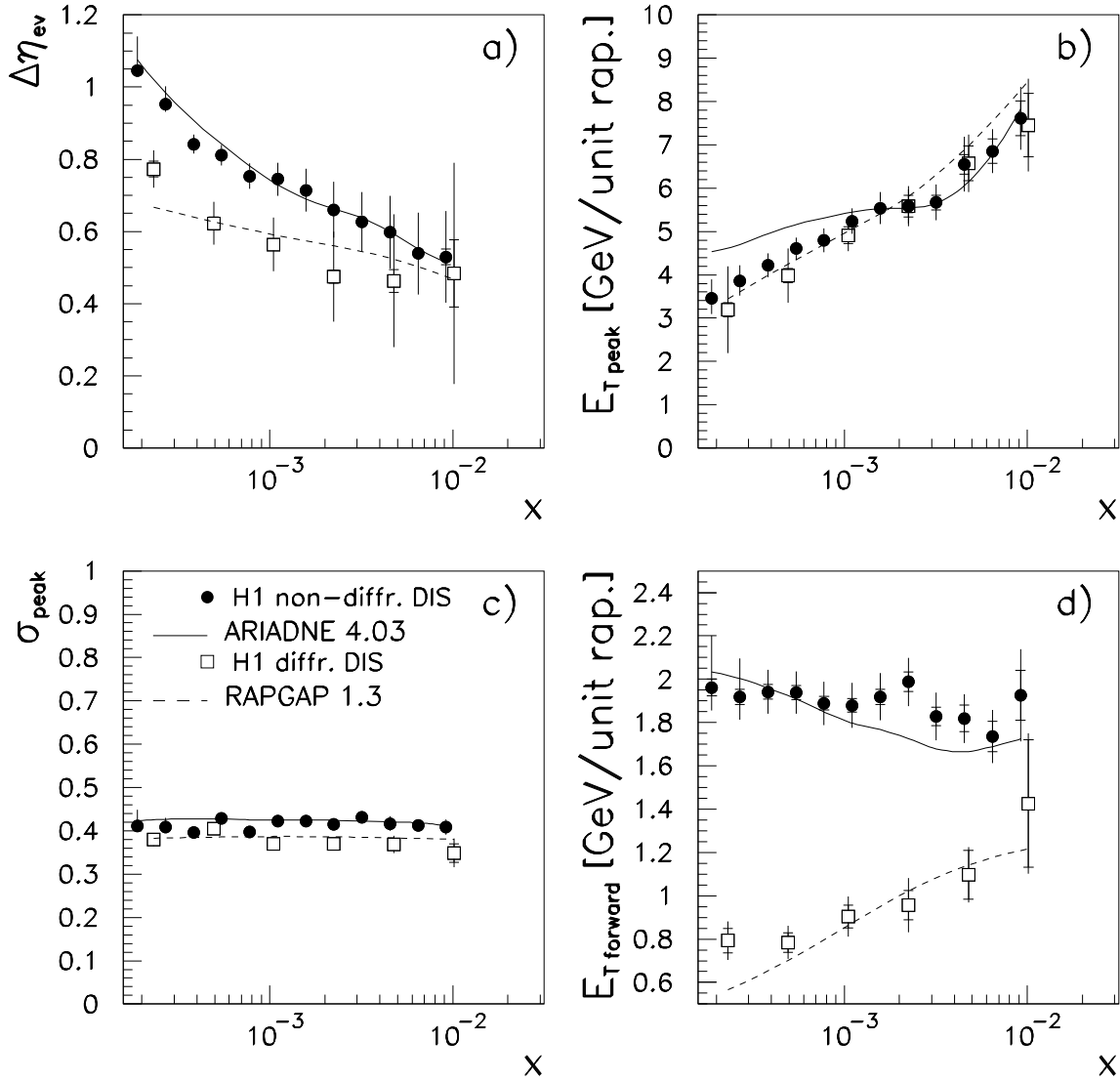


Figure 3: Measured estimators of the transverse energy flow for non-diffractive (“non-diffr. DIS”) and diffractive (“diffr. DIS”) DIS, compared with the ARIADNE and RAPGAP models. Shown is the dependence on x for the measured deviation from the calculated direction (a), for the magnitude of the current region (b), for the width of the current region (c) and for the forward transverse energy (d).

DIS the measured value is found to be smaller by about 0.2 units in pseudo-rapidity than in the case of non-diffractive DIS. $E_{T\ peak}$ increases with increasing values of x with no difference visible between the two classes. No x -dependence is observed for $\sigma_{\ peak}$ which has a value of ≈ 0.4 (this corresponds to a full-width-half-maximum for a Gaussian shaped distribution of about 0.9). Significant differences are observed in $E_{T\ forward}$, where for non-diffractive data $E_{T\ forward} \approx 2$ GeV/unit-of-rapidity with almost no dependence on x . For the diffractive case $E_{T\ forward}$ increases with increasing values of x , the magnitude being lower by 20 – 60 % compared with non-diffractive DIS, as expected and demonstrated clearly in the following. Also shown are the predictions of the models (ARIADNE 4.03 and RAPGAP 1.3) that have been used to correct for detector effects. The data are described reasonably well for both cases. At small values of x ($< 10^{-3}$) the ARIADNE model (version 4.03) overestimates the measured values of $E_{T\ peak}$.

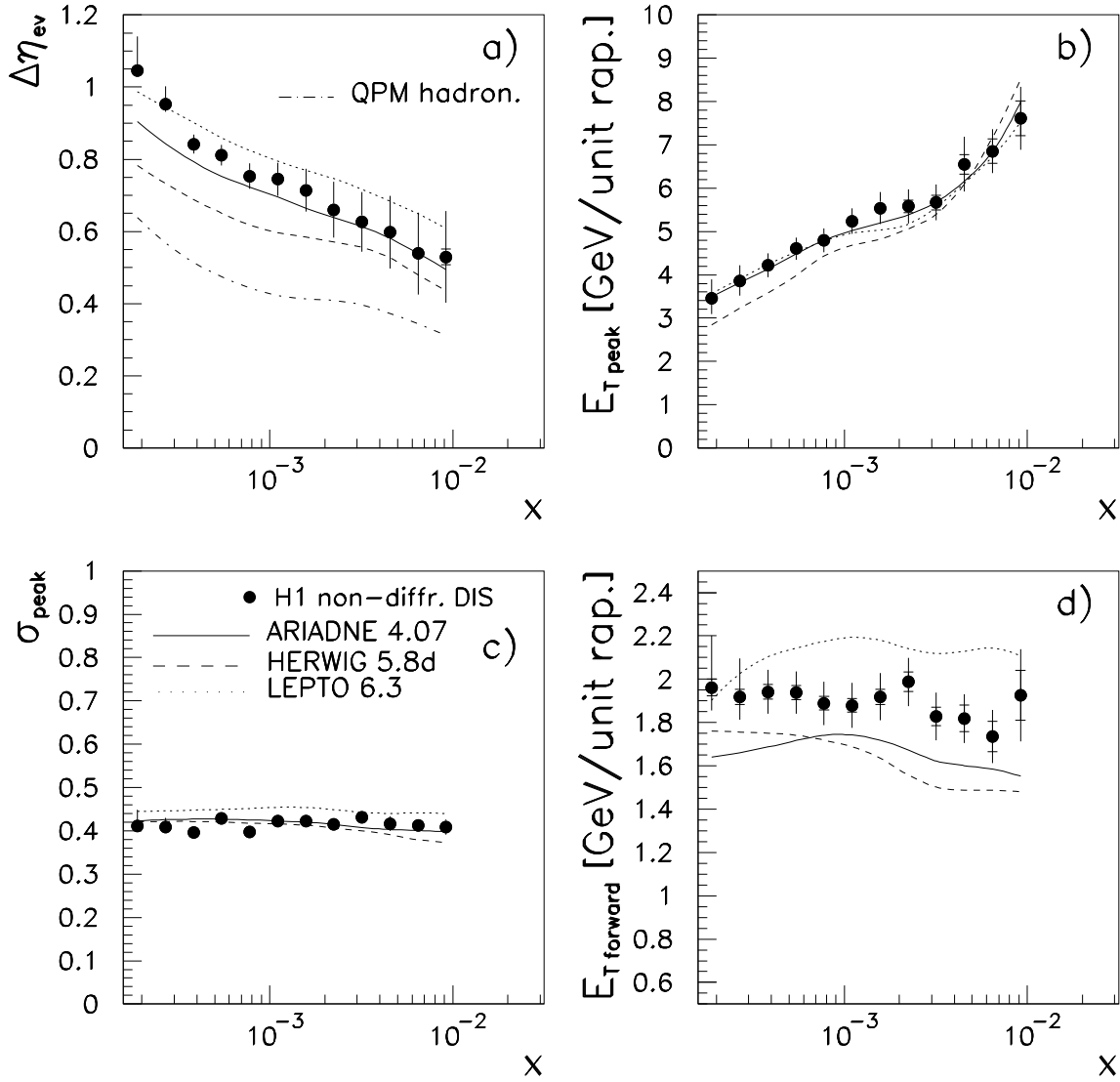


Figure 4: Measured dependence of the estimators on x for non-diffractive DIS, compared with the prediction of the ARIADNE 4.07, HERWIG 5.8d and LEPTO 6.3 models. Shown are the measured deviation from the calculated direction (a), the magnitude of the current region (b), the width of the current region (c) and the forward transverse energy (d). In addition a QPM calculation including hadronization is shown in (a).

Decreasing values of x correspond on average to an increase in the invariant mass W of the hadronic system. This is expected to lead to an increase of the phase space for effects of perturbative QCD and particle production in the final state. The measured deviation from the naïve QPM expectation is sensitive to this increase and also to details of the implementation of QCD effects in the different models. In a previous analysis[21] it has been shown that the level of transverse energy in the central region of the γ^*p system (this corresponds to the forward region in the laboratory frame) increases with decreasing x for constant Q^2 .

Before investigating in more detail the diffractive contribution, some recent versions of models for DIS will be compared with non-diffractive data. The development of these versions of the models was motivated by the previously unsatisfactory description of the measured hadronic final state for $x < 10^{-3}$ as shown in[21, 28]. The comparison of the predictions of ARIADNE (version 4.07), HERWIG (version

5.8d) and LEPTO (version 6.3) with the measured data in figure 4 shows clear deviations, the differences being most pronounced in the estimators for $\Delta\eta_{ev}$ and E_{Tforw} . The shape of the dependence of $\Delta\eta_{ev}$ is very similar for these three models but not as steep at small x as in the data. The predicted shape and the magnitude of the E_{Tforw} dependence on x differs between models. The description of the data obtained with these models is in general worse than that given by version (4.03) of ARIADNE (figure 3). In figure 4 (a) also a QPM like calculation for the final state is shown. For this calculation (done with the LEPTO model) only the contribution from the Born term for DIS was considered together with hadronization as implemented in the Lund string model. For all values of x this calculation significantly underestimates the measured deviation. It should be noted that a pure Born term calculation at the parton level (i.e. no hadronization) gives $\Delta\eta_{ev} = 0$. This underlines the well known need to include effects of perturbative QCD (i.e. emission of gluons) in the modelling of the hadronic final state. However the understanding of the final state in the new kinematic domain of DIS opened by HERA ($x < 10^{-3}$) still remains a challenge.

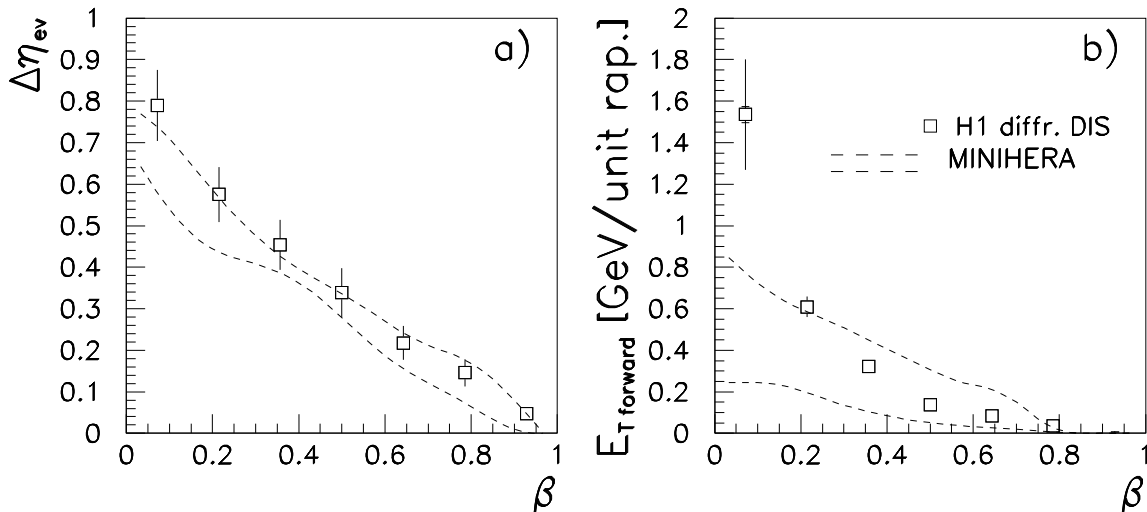


Figure 5: Measured estimators for diffractive DIS, compared with a model calculation for ep collisions with a reduced proton beam energy. The dashed lines indicate the range of the MINIHERA prediction for energies between 0.82 GeV and 8.2 GeV. Shown is the dependence on β (x for the MINIHERA model) for the measured deviation from the calculated direction (a) and for the forward transverse energy (b).

The properties of diffractive DIS are now investigated in more detail. As the phase space for hadron production depends on the invariant mass of the final state, is expected that a large part of the differences in the E_T flow observed in the diffractive and non-diffractive case are due to the fact that in diffractive DIS there is an isolated leading colourless remnant. This expectation is tested by comparing a model calculation (called “MINIHERA”) for deep-inelastic scattering of 26.7 GeV electrons and $f \cdot 820$ GeV protons to the diffractive data. For a value of $f = 0.003$ the average values of W_{MINIHERA}^2 and M_X^2 (in the diffractive data) are about equal ($\approx 80 \text{ GeV}^2$). This corresponds to the average value of x_P in the data (i.e. the average momentum of the pomeron using the picture of figure 1). To estimate the effect of the spread in x_P as in the measurements, the calculation was done at the values $f = 0.001$ and $f = 0.01$. For all the calculations the ARIADNE model (version 4.03) was used with all other parameters identical to those used in the calculations for the nominal HERA conditions. The results were cross-checked by a calculation with LEPTO (version 6.1) which leads to the same conclusions.

Figure 5 shows the β dependence of the two estimators $\Delta\eta_{ev}$ and E_{Tforw} for the diffractive data.

Both estimators show a strong increase with decreasing values of β which corresponds to x in DIS. Low values of β correspond to large masses M_X of the γ^*P system. The limit $\beta \rightarrow 1$ corresponds to $M_X \rightarrow 0$ which means that the available phase space vanishes completely. The dependence of $\Delta\eta_{ev}$ on β in the diffractive data is described reasonably well by the MINHERA model calculation, whereas the E_{Tforw} dependence is significantly underestimated for values of $\beta < 0.2$. This calculation is used only to demonstrate the effect on the production of hadrons given the different invariant mass of the final state in the diffractive data when compared to the non-diffractive data. The obvious limitations of the calculation are the fact that the target is simply chosen to be a proton and furthermore a fixed value of f (corresponding to x_P) is used, in contrast to the x_P distribution in the data. However it can be concluded that the differences observed between the two classes of DIS data (figure 3) can be interpreted as a result of the differences in the available phase space for hadron production in the final state. More meaningful quantitative comparisons of a model of diffraction are made in the following. In this model the incident electron probes a pomeron with a more realistic partonic content, and therefore some of these shortfalls do not occur.

In figure 6 the dependence of $\Delta\eta_{ev}$ and E_{Tforw} on x_P is shown together with the dependence on β (as shown in figure 5) for diffractive DIS. The corresponding values are listed in tables 3 and 4 in the appendix. The measured deviation $\Delta\eta_{ev}$ is observed to increase moderately whereas E_{Tforw} strongly increases with increasing values of x_P , as is to be expected as the isolation of the colourless remnant in diffraction from other hadrons is reduced.

Also shown are the predictions of three models which can generate a diffractive contribution to DIS. RAPGAP (version 1.3) is able to give a good description of the data over the whole range in x_P and β . Here diffractive DIS is modelled as deep-inelastic electron scattering of a partonic constituent of a pomeron, the latter being emitted from the proton. In the evolution of the final state, perturbative QCD effects are taken into account. A QPM like calculation is also shown. This calculation was performed with the RAPGAP model, considering only the Born term (i.e. electron-quark scattering) and subsequent fragmentation via the Lund string model. This calculation is observed to underestimate the data considerably in kinematic regions ($\beta < 0.3$ or $x_P > 0.01$) which corresponds to larger values of M_X and thus indicates the need to include effects of perturbative QCD for diffractive DIS as well. Compared to RAPGAP the other two models give a worse description of the data, reproducing neither the shape nor the magnitude of the measurements correctly. It should be noted that these discrepancies can be correlated with the unsatisfactory description of the non-diffractive final state in these models.

A previous analysis[11] by the ZEUS collaboration comparing the energy flow $\frac{dE}{d\Delta\eta}$ relative to the naïve QPM expectation found at most a small deviation from this expectation for events with a LRG and a maximum value of the deviation of about 0.4 in $\Delta\eta$ for events without a gap. In the analysis presented here significant deviations from the QPM expectation are observed for both classes of DIS events. This is due to the choice of E_T as the weight for the pseudo-rapidity distribution relative to the expected QPM direction. Using E_T rather than E as weighting factor leads to a greater sensitivity to deviations from the QPM expectation for low values of x .

As demonstrated above, the reduction of the phase space available for the final state in the case of diffractive DIS is the main reason for the observed differences compared with the non-diffractive case. This conclusion was recently also reached by the ZEUS collaboration in[12], where charged particle spectra in DIS have been analyzed in the current region of the γ^*p centre of mass system. A comparison of the measured transverse momenta with data from fixed target experiments at a value of W comparable to M_X in the LRG events gave good agreement.

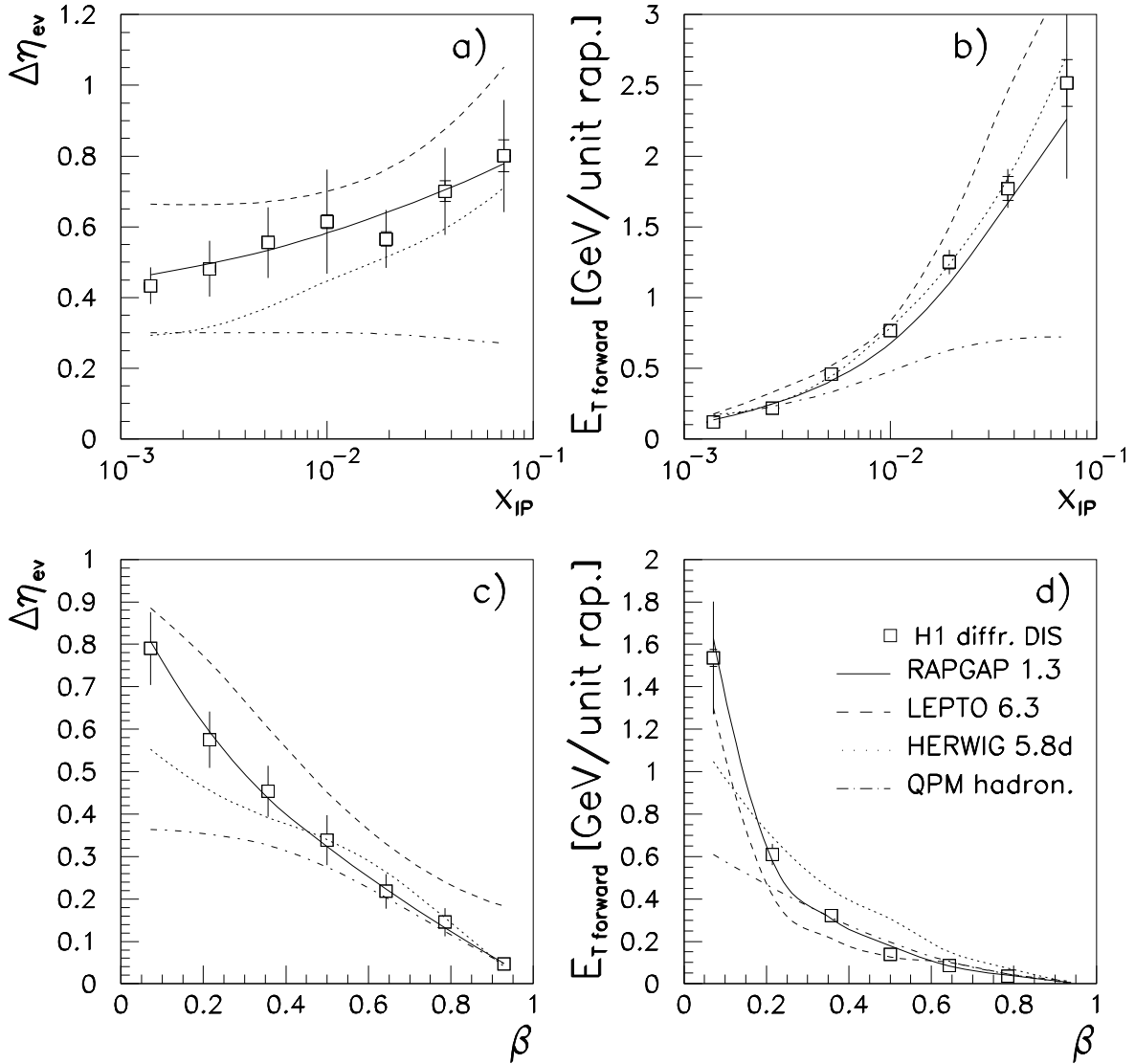


Figure 6: Measured estimators for diffractive DIS compared with several different models. Shown is the dependence on x_P for the measured deviation from the calculated direction (a) and for the forward transverse energy (b) as well as the dependence on β for the deviation (c) and for the forward transverse energy (d). In addition a QPM calculation including hadronization is shown.

8 Summary and Conclusions

Measurements of transverse energy flow E_T in deep-inelastic ep scattering have been made using data taken at HERA with the H1 experiment. The energy flow was analyzed in the laboratory frame of reference for diffractive and non-diffractive data. The diffractive data are selected experimentally by demanding a large rapidity gap in the hadronic final state around the proton remnant direction, making measurements of diffraction possible in the range $x < x_P < 0.02$. Estimators which quantify features of the topology of the E_T flow, corrected for detector effects, have been compared with the expectations of different models based on QCD.

The measurements indicate that the interpretation of deep-inelastic scattering as the scattering of a current quark with associated effects of perturbative QCD continues to be valid for the hadronic final

state of the diffractive process. The level at which these effects occur is consistent with the reduced phase space available in the diffractive process compared to that in non-diffractive DIS.

The measured E_T flow for diffractive DIS is well described by a model (RAPGAP), in which the proton couples at low momentum transfer squared t to a colourless object (pomeron). Here the deep-inelastic scattering process involves the partonic structure of the pomeron.

Models for deep-inelastic ep scattering (LEPTO and HERWIG) in which the interaction of the electron involves the partonic structure of the proton, and not the one of an entity such as the pomeron, have been investigated. Here the diffractive configuration occurs because of non-perturbative QCD effects in the formation of the final state. These models do not describe the measurements of E_T flow in diffractive DIS as well as RAPGAP. The observed discrepancies are however at a level which is similar to the disagreement observed for the bulk of DIS data, and therefore it is possible that further developments in these models may rectify this disagreement.

Acknowledgments. We are very grateful to the HERA machine group whose outstanding efforts made this experiment possible. We acknowledge the support of the DESY technical staff. We appreciate the big effort of the engineers and technicians who constructed and maintained the detector. We thank the funding agencies for financial support of this experiment. We wish to thank the DESY directorate for the hospitality extended to the non-DESY members of the collaboration.

Appendix

$\log_{10}x$	$\Delta\eta_{ev}[\text{rapidity}]$	$E_{T\text{peak}}[\text{GeV}/\text{rapidity}]$	$\sigma_{\text{peak}}[\text{rapidity}]$	$E_{T\text{forw}}[\text{GeV}/\text{rapidity}]$
-3.72	$1.05 \pm 0.01 \begin{smallmatrix} +0.09 \\ -0.01 \end{smallmatrix}$	$3.5 \pm 0.1 \begin{smallmatrix} +0.4 \\ -0.3 \end{smallmatrix}$	$0.41 \pm 0.01 \begin{smallmatrix} +0.04 \\ -0.01 \end{smallmatrix}$	$1.96 \pm 0.04 \begin{smallmatrix} +0.20 \\ -0.10 \end{smallmatrix}$
-3.57	$0.95 \pm 0.01 \begin{smallmatrix} +0.05 \\ -0.02 \end{smallmatrix}$	$3.9 \pm 0.1 \begin{smallmatrix} +0.4 \\ -0.3 \end{smallmatrix}$	$0.41 \pm 0.01 \begin{smallmatrix} +0.02 \\ -0.01 \end{smallmatrix}$	$1.92 \pm 0.03 \begin{smallmatrix} +0.14 \\ -0.10 \end{smallmatrix}$
-3.42	$0.84 \pm 0.01 \pm 0.02$	$4.2 \pm 0.1 \pm 0.3$	$0.40 \pm 0.01 \pm 0.01$	$1.94 \pm 0.03 \pm 0.10$
-3.26	$0.81 \pm 0.01 \pm 0.03$	$4.6 \pm 0.1 \pm 0.2$	$0.43 \pm 0.01 \pm 0.01$	$1.94 \pm 0.03 \pm 0.09$
-3.11	$0.75 \pm 0.01 \pm 0.03$	$4.8 \pm 0.1 \pm 0.3$	$0.40 \pm 0.01 \pm 0.01$	$1.89 \pm 0.03 \pm 0.10$
-2.96	$0.75 \pm 0.01 \pm 0.05$	$5.2 \pm 0.1 \pm 0.3$	$0.42 \pm 0.01 \pm 0.01$	$1.88 \pm 0.03 \pm 0.10$
-2.80	$0.71 \pm 0.01 \pm 0.06$	$5.5 \pm 0.1 \pm 0.3$	$0.42 \pm 0.01 \pm 0.01$	$1.92 \pm 0.04 \pm 0.10$
-2.65	$0.66 \pm 0.01 \pm 0.08$	$5.6 \pm 0.2 \pm 0.4$	$0.42 \pm 0.01 \pm 0.01$	$1.99 \pm 0.05 \pm 0.10$
-2.50	$0.63 \pm 0.01 \pm 0.08$	$5.7 \pm 0.2 \pm 0.4$	$0.43 \pm 0.01 \pm 0.01$	$1.83 \pm 0.04 \pm 0.10$
-2.34	$0.60 \pm 0.01 \pm 0.10$	$6.6 \pm 0.2 \pm 0.6$	$0.42 \pm 0.01 \pm 0.02$	$1.82 \pm 0.06 \pm 0.09$
-2.19	$0.54 \pm 0.02 \pm 0.11$	$6.9 \pm 0.3 \pm 0.4$	$0.41 \pm 0.01 \pm 0.01$	$1.74 \pm 0.07 \pm 0.10$
-2.04	$0.53 \pm 0.02 \pm 0.13$	$7.6 \pm 0.4 \pm 0.6$	$0.41 \pm 0.01 \pm 0.02$	$1.93 \pm 0.12 \pm 0.18$

Table 1: Values of the energy flow estimators as a function of x for non-diffractive DIS. The first error given is the statistical, the second is the systematic error.

$\log_{10}x$	$\Delta\eta_{ev}[\text{rapidity}]$	$E_{T_{peak}}[\text{GeV}/\text{rapidity}]$	$\sigma_{peak}[\text{rapidity}]$	$E_{T_{forw}}[\text{GeV}/\text{rapidity}]$
-3.64	$0.77 \pm 0.02 \pm 0.05$	$3.2 \pm 0.2 \pm 1.0$	$0.38 \pm 0.01 \pm 0.01$	$0.79 \pm 0.06 \pm 0.07$
-3.31	$0.62 \pm 0.02 \pm 0.06$	$4.0 \pm 0.2 \pm 0.6$	$0.41 \pm 0.01 \pm 0.01$	$0.78 \pm 0.05 \pm 0.06$
-2.98	$0.56 \pm 0.02 \pm 0.07$	$4.9 \pm 0.2 \pm 0.3$	$0.37 \pm 0.01 \pm 0.01$	$0.90 \pm 0.05 \pm 0.08$
-2.65	$0.48 \pm 0.02 \pm 0.12$	$5.6 \pm 0.3 \pm 0.4$	$0.37 \pm 0.01 \pm 0.01$	$0.96 \pm 0.07 \pm 0.11$
-2.32	$0.46 \pm 0.03 \pm 0.18$	$6.6 \pm 0.4 \pm 0.5$	$0.37 \pm 0.01 \pm 0.02$	$1.10 \pm 0.11 \pm 0.06$
-1.99	$0.48 \pm 0.09 \pm 0.29$	$7.5 \pm 0.7 \pm 0.8$	$0.35 \pm 0.02 \pm 0.03$	$1.43 \pm 0.30 \pm 0.13$

Table 2: Values of the energy flow estimators as a function of x for diffractive DIS. The first error given is the statistical, the second is the systematic error.

$\log_{10}x_{\mathcal{P}}$	$\Delta\eta_{ev}[\text{rapidity}]$	$E_{T_{forw}}[\text{GeV}/\text{rapidity}]$
-2.86	$0.43 \pm 0.01 \pm 0.05$	$0.12 \pm 0.01 \pm 0.02$
-2.57	$0.48 \pm 0.01 \pm 0.08$	$0.22 \pm 0.01 \pm 0.02$
-2.29	$0.56 \pm 0.02 \pm 0.10$	$0.46 \pm 0.02 \pm 0.03$
-2.00	$0.61 \pm 0.02 \pm 0.15$	$0.77 \pm 0.03 \pm 0.04$
-1.71	$0.57 \pm 0.02 \pm 0.08$	$1.25 \pm 0.05 \pm 0.07$
-1.43	$0.70 \pm 0.03 \pm 0.12$	$1.77 \pm 0.09 \pm 0.11$
-1.14	$0.80 \pm 0.05 \pm 0.15$	$2.52 \pm 0.17 \pm 0.66$

Table 3: Values of the energy flow estimators as a function of $x_{\mathcal{P}}$ for diffractive DIS. The first error given is the statistical, the second is the systematic error.

β	$\Delta\eta_{ev}[\text{rapidity}]$	$E_{T_{forw}}[\text{GeV}/\text{rapidity}]$
0.07	$0.79 \pm 0.01 \pm 0.09$	$1.54 \pm 0.04 \pm 0.26$
0.21	$0.58 \pm 0.01 \pm 0.07$	$0.61 \pm 0.02 \pm 0.05$
0.36	$0.45 \pm 0.01 \pm 0.06$	$0.32 \pm 0.01 \pm 0.01$
0.50	$0.34 \pm 0.01 \pm 0.06$	$0.14 \pm 0.01 \pm 0.01$
0.64	$0.23 \pm 0.01 \pm 0.04$	$0.09 \pm 0.01 \pm 0.01$
0.79	$0.15 \pm 0.01 \pm 0.03$	$0.04 \pm 0.01 \pm 0.01$
0.93	$0.05 \pm 0.01 \pm 0.01$	$0.01 \pm 0.01 \pm 0.01$

Table 4: Values of the energy flow estimators as a function of β for diffractive DIS. The first error given is the statistical, the second is the systematic error.

References

- [1] S. Bethke and J.E. Pilcher, *Ann. Rev. of Nucl. and Part. Sci.* 42 (1992) 251.
- [2] J.E. Huth and M.L. Mangano, *Ann. Rev. of Nucl. and Part. Sci.* 43 (1993) 585.
- [3] S.R. Mishra and F. Sciulli, *Ann. Rev. of Nucl. and Part. Sci.* 39 (1989) 259.
- [4] K. Goulianos, *Phys. Rep.* 101 (1983) 169.
- [5] G. Ingelman and P.E. Schlein, *Phys. Lett. B* 152 (1985) 256.
- [6] UA8 Collaboration, R. Bonino et al., *Phys. Lett. B* 211 (1988) 239.
- [7] ZEUS Collaboration, M.Derrick et al., *Phys. Lett. B* 315 (1993) 481.
- [8] H1 Collaboration, T. Ahmed et al., *Nucl. Phys. B* 429 (1994) 477.
- [9] H1 Collaboration, T. Ahmed et al., *Phys. Lett. B* 348 (1995) 681.
- [10] ZEUS Collaboration, M.Derrick et al., *Z. Phys C* 68 (1995) 569.
- [11] ZEUS Collaboration, M. Derrick et al., *Phys. Lett. B* 338 (1994) 483.
- [12] ZEUS Collaboration, M. Derrick et al., *Inclusive Charged Particle Distributions in Deep Inelastic Scattering Events at HERA*, DESY preprint 95-221.
- [13] H. Jung, *Comp. Phys. Comm.* 86 (1995), 147.
- [14] G. Ingelman, *LEPTO Version 6.1: The Lund Monte Carlo for Deep Inelastic Lepton–Nucleon Scattering*, Proc. of the Workshop on Physics at HERA, Hamburg 1991, eds. W. Buchmüller and G. Ingelman, vol. 3, p. 1366.
- [15] M. Seymour, *Comp. Phys. Comm.* 67 (1992), 465.
- [16] H1 Collaboration, T. Ahmed et al., *The H1 detector at HERA*, DESY preprint 93–103 (1993).
- [17] H1 Calorimeter Group, B. Andrieu et al., *Nucl. Inst. Meth. A* 336 (1993) 460.
- [18] H1 Calorimeter Group, B. Andrieu et al., *Nucl. Inst. Meth. A* 336 (1993) 499, *ibid. A* 350 (1994) 57.
- [19] H1 Collaboration, T. Ahmed et al., *Nucl. Phys. B* 439 (1995) 471.
- [20] H1 Collaboration, T. Ahmed et al., *Z. Phys. C* 63 (1994) 377.
- [21] H1 Collaboration, S. Aid et al., *Phys. Lett. B* 356 (1995), 118.
- [22] V.N. Gribov and L.N. Lipatov, *Sov. J. Nucl. Phys.* 15 (1972) 438 and 675,
G. Altarelli and G. Parisi, *Nucl. Phys. B* 126 (1977) 298,
Yu.L. Dokshitzer, *Sov. Phys. JETP* 46 (1971) 641.
- [23] B. Andersson et al., *Phys. Rep.* 97 (1983) 31.
- [24] T. Sjöstrand, *Comp. Phys. Comm.* 82 (1994) 74.
- [25] A. Edin, G. Ingelman and J. Rathsmann, *Rapidity Gaps in DIS Through Soft Colour Interactions*, Talk given at Workshop on Deep Inelastic Scattering and QCD (DIS 95), Paris, France, 24–28 Apr 1995.
- [26] W. Buchmueller and A. Hebecker, *Phys. Lett. B* 355 (1995) 573.

- [27] L. Lönnblad, *Comp. Phys. Comm.* 71 (1992) 15.
- [28] H1 Collaboration, S. Aid et al., *Phys. Lett. B* 358 (1995) 412.
- [29] B. Andersson, G. Gustafson and L. Lönnblad, *Nucl. Phys. B* 339 (1990) 393.
- [30] L. Lönnblad, *Reconnecting Coloured Dipoles*, CERN preprint TH/95-218.
- [31] M. Seymour and J. Chyla, *private communication*.
- [32] A.D. Martin, W.J. Stirling and R.G. Roberts, *MRS Parton Distributions*, Proc. of the Workshop on Quantum Field Theory Theoretical Aspects of High Energy Physics, eds. B. Geyser and E.M. Ilgenfritz (1993), p. 11.
- [33] H1 Collaboration, T. Ahmed et al., *Phys. Lett. B* 407 (1993) 515.
- [34] ZEUS Collaboration, M. Derrick et al., *Phys. Lett. B* 316 (1993), 412.
- [35] K. Charchula, G. Schuler and H. Spiesberger, *Comp. Phys. Comm.* 81 (1994), 381.